Intercalative Polymerization of L-Lactide with Organically Modified Clay by a Reactive Extrusion Method and Instrumental Analyses of the Poly(lactic acid)/Clay Nanocomposites

Masakazu Nishida,[1] Toshiyuki Tanaka,[2] Tomohiro Yamaguchi,[3] Kenzi Suzuki,[4] Wataru Kanematsu[1]

[1]*National Institute of Advanced Industrial Science and Technology, 2266-98 Shimoshidami, Moriyama-Ku, 463-8560 Nagoya, Japan*
[2]*Mikawa Textile Research Center, Aichi Center for Industry and Science Technology, 109 Igakubo, Otsuka-Cho, 443-0013 Gamagori, Japan*
[3]*Industrial Research Center, Aichi Center for Industry and Science Technology, 1-157-1 Onda-Cho, 448-0013 Kariya, Japan*
[4]*Department of Chemical Engineering, Graduate School of Engineering, Nagoya University, Furo-Cho, Chikusa-Ku, 464-8603 Nagoya, Japan*

Received 30 June 2010; accepted 22 November 2011
DOI 10.1002/app.36530
Published online 17 February 2012 in Wiley Online Library (wileyonlinelibrary.com).

ABSTRACT: Using a reactive extrusion-molding process, we produced poly(lactic acid) (PLA) nanocomposites from L-lactide monomer in the presence of organic montmorillonites. On the basis of X-ray diffraction, scanning electron microscopy, and transmission electron microscopy analyses, we determined that the intercalation of the PLA between the clay layers in the mixing process, followed by disappearance of agglomeration, proceeded in the extrusion process. Although only a slight change in the chemical shifts in cross-polarization/magic angle spinning ^{13}C-NMR was observed with the addition of the organic clay, the presence of the additive and the organic content of the nanocomposites affected the nuclear magnetic relaxation times [the ^{1}H spin-lattice relaxation time (T_1H) and the ^{13}C spin-lattice relaxation time (T_1C)] for different temperatures. The nanoclay suppressed increases in T_1H at elevated temperatures and extended T_1C values of C=O and CH around room temperature. © 2012 Wiley Periodicals, Inc. J Appl Polym Sci 125: E681–E690, 2012

Key words: electron microscopy; nanocomposites; NMR; polyesters; reactive extrusion

INTRODUCTION

In recent years, new polymer/nanoclay systems have been studied to give additional functions to biodegradable polymers such as poly(lactic acid) (PLA).[1] These polymer/nanoclay systems consist of layered silicate nanosized fillers and show three types of morphology, microcomposite, intercalated, and exfoliated, depending on the clay type and the production methods.[2] The alternation of the morphology induces various superior properties, such as stiffness, permeability, crystallinity, and thermal stability. In functionalizing nanoclay composite systems, 2 : 1 layered phyllosilicates have been found to be appropriate for controlling a highly ordered structure. These approaches for producing polymer/nanoclay systems are effective for PLA/nanoclay systems, and several interesting studies of these systems have been surveyed.[3–5] The production methods of PLA/clay nanocomposites may be divided into two main categories: nanodispersion of the clay in the polymer matrix and polymerization in the presence of the nanosized fillers.

The preparation of PLA/clay nanocomposite starting from PLA pellets with organically modified montmorillonite by the melt-mixing method with a corotating twin-screw extruder is the most established method.[6] This method has been applied to the preparation of PLA/clay nanocomposite consisting of organically modified smectite,[2] mica,[7] and rectorite.[8] Plasticized PLA/clay nanocomposites have also been obtained by the melt-mixing method with a corotating twin-screw extruder[9] and the direct melt-blending method.[10] Furthermore, exfoliated PLA/clay nanocomposites have been prepared in chloroform[11] and in tetrahydrofuran.[12]

On the other hand, in the production method that uses polymerization from L-lactide with nanosized fillers, both intercalated and exfoliated PLA/clay nanocomposites have been prepared by the *in situ*

Correspondence to: M. Nishida (m-nishida@aist.go.jp).
Contract grant sponsor: Innovation Plaza Tokai of Japan Science and Technology Agency.

coordinative polymerization of L-lactide with bulk polymerization. These processes also yielded nanocomposites with high clay contents, which were used as a masterbatches for subsequent compounding.[13,14] To our knowledge, however, few reports have been published on the *in situ* preparation of PLA/clay nanocomposites by melt-mixing with single- or twin-screw extruders, although some works have been carried out on the bulk polymerization of L-lactide and the block copolymerization of poly(L-lactide) and poly(ε-caprolactone) or poly(ethylene glycol) with and without a reactive extruder.[15,16]

For this study, we assembled a new type of reactive extrusion-molding machine with a mixing screw placed at the hopper of a single-screw extruder. This machine facilitated the processes of simultaneous polymerization and molding to provide materials in the shapes of fibers and films starting from monomers and/or polymers. In a previous article, we reported that clay/polystyrene–polybutadiene–polystyrene triblock copolymer intercalated nanocomposites were prepared with an organoclay containing stearic acid by melt blending.[17] We also reported that by the reaction of a pristine montmorillonite with distearyldimethylammonium (D18) cation, an organically modified montmorillonite by D18 cation-exchange (D18Mt) material was prepared and melt-blended with polystyrene–poly(ethylene-*co*-butylene)–polystyrene triblock copolymer (SEBS) to provide clay/SEBS intercalated composites; the resulting material exhibited an improved tensile modulus, tear strength, and hardness.[18] In this study, with reactive extrusion molding, the coordination polymerization of L-lactide monomer was examined in the presence of organically modified montmorillonite (D18Mt). The characterization of the resulting material revealed the formation of a PLA/clay nanocomposite with an intercalated morphology. We also discuss the structures and mobilities of these intercalated PLA/clay nanocomposites with a focus on relaxation analyses with the solid-state NMR method.

EXPERIMENTAL

Materials

Montmorillonite (Kunipia-F) was obtained from Kunimine Industries (Tokyo, Japan). The cation-exchange capacity of the sample was 115 mequiv/100 g. D18 chloride, used as a surface modifier, was purchased from Tokyo Chemical Industry (Tokyo, Japan). Industrial-grade L-lactide (L content = 88%) was purchased from Musashino Chemical Laboratory (Tokyo, Japan) and was used without further purification. Tin 2-ethylhaxanoate [$Sn(Oct)_2$] was purchased from Wako Pure Chemical Industries (Osaka, Japan) and was used as a catalyst. Irganox 1010 was purchased from Chiba Japan Co. (Tokyo, Japan) and was used as an antioxidant for the polymer products. Pelletized poly(L-lactic acid) (PLA_ref) was purchased from Mitsui Chemicals (Tokyo, Japan) [number-average molecular weight (M_n) = 98,000, glass-transition temperature (T_g) = 60°C].

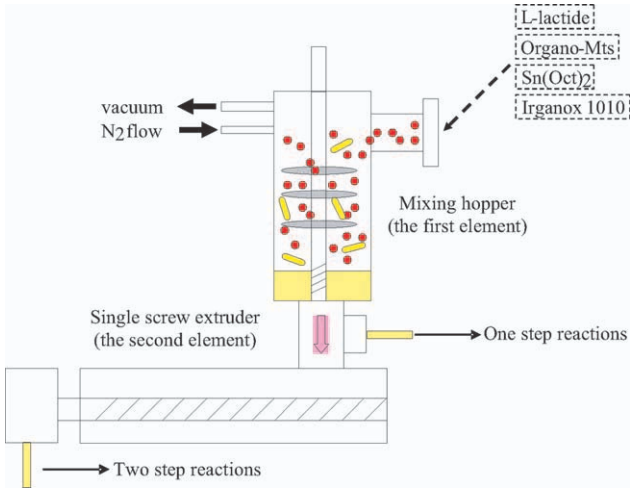

Figure 1 Diagram of the reactive extrusion-molding machine. [Color figure can be viewed in the online issue, which is available at wileyonlinelibrary.com.]

Preparation of the organically modified montmorillonite

Organomontmorillonites (organo-Mts) with different amounts of D18 were prepared during previous studies.[18] The differing amounts of D18 in the organo-Mts gave exchanged cation rates of 60, 80, and 100%, and the products were labeled D18Mt(60), D18Mt(80), and D18Mt(100), respectively. The apparent organic contents of D18Mt(60), D18Mt(80), and D18Mt(100), which were calculated from the weights before and after heating at 1000°C for 1 h, were 35.5, 40.8, and 45.8 wt %, respectively. The organo-Mts were dried at 80 °C overnight *in vacuo* before polymerization to minimize the influence of water.

Typical procedure of melt polymerization with the reactive extrusion equipment

The melt polymerization of L-lactide with organo-Mts was performed with the reactive extrusion machine, as shown in Figure 1. A 300-g sample of industrial-grade L-lactide was placed in a 500-mL beaker; this was followed by the addition of 3 wt % of the dried D18Mt(80), 0.3 wt % of $Sn(Oct)_2$, and 0.3 wt % of Irganox 1010; the sample in the beaker was then gently mixed by hand. These samples were put into the mixing hopper part of the reactive extrusion-molding machine. With heating at 120 °C under a nitrogen atmosphere, the samples were stirred by a shuttlecock-type screw at 6 rpm for 60 min and were then stirred *in vacuo* at 170 °C for 30 min. Through a gear pump

equipped under the mixing hopper with a nitrogen flow, the melting mixture was introduced into the single-screw chamber of the reactive extrusion machine. With heating at 160–180 °C, the melting mixture was extruded at a rotation speed of 5 rpm. The melted polymer composite was ejected from a spinning disc located at the extruder exit into water at ambient temperature to provide a solidified fiber. Small amounts of unreacted L-lactide and existing water in the system were recovered in a trap equipped on the vacuum pump. For some samples, the polymer was taken from a collection entrance under the gear pump and immersed into water to give a solidified mass.

Characterization of the PLA/clay nanocomposites

The nanocomposite samples were analyzed with gel permeation chromatography at 40 °C with a Tosoh (Tokyo, Japan) GPC-H8020 instrument equipped with a Tosoh TSKgel GMH_{HR}-M column and a differential refractometer detector. Chloroform was used as the eluent at a flow rate of 1.0 mL/min, and the molecular weights were calibrated with polystyrene standards.

The differential scanning calorimetry (DSC) data for the samples were recorded on a Rigaku-Denki TAS-100 (Tokyo, Japan). Pure PLA and composite samples of 5 mg were heated at a rate of 10 K/min under a nitrogen atmosphere over a temperature range of 0–250 °C to measure their T_g, crystallization temperature (T_c), and melting temperature (T_m) values. Thermogravimetric analysis (TGA) was performed on the Rigaku-Denki TAS-100 to provide the thermal decomposition temperature (T_{dec}).

X-ray powder diffractometry was performed with a Rigaku-Denki RINT-2000 and RINT-2200 diffractometer equipped with a Cu Kα ($\lambda = 0.14$ nm) source in the 2θ range 0.84–30 ° at a scan speed of 2.0/min. Tensile properties of the fibers were measured with a Tensilon system (RTC-1250, Orientec Co., Tokyo, Japan), at 20 °C and a relative humidity of 65%, where the crosshead speed was set at 20 mm/min and the length of specimens was 20 mm. All of the tensile properties given in this article represent average values of five trials. Scanning electron microscopy (SEM) images were recorded with a JEOL JST-5310 (Tokyo, Japan) at an acceleration voltage of 15 kV. Transmission electron microscopy (TEM) images were recorded with a JEOL JEM-1400EX at an acceleration voltage of 100 kV. Ultrathin sections (70 nm) of the nanocomposites were prepared in epoxy resin by a Leica ULTRACUT instrument (Wetzlar, Germany) at ambient temperature. The sections were transferred from water to 200-mesh Cu grids and were then carbon-coated.

NMR measurements

The ^{1}H-NMR spectra were measured with $CDCl_3$ as the solvent on a Varian INOVA-300 spectrometer (Palo Alto, CA) operated at 299.96 MHz with a Varian 5-mm four-nucleus auto-NMR triple-resonance liquid probe for the ^{1}H nuclei and a 3.74-s acquisition period with a 7.0-μs $\pi/2$ pulse for the ^{1}H nuclei. The spectra were collected over a 4.5-kHz spectral width with a 1.2-s recycle delay in 16 transients.

The solid-state ^{13}C-NMR spectra were measured on a Varian 400 NMR system spectrometer operated at 100.56 MHz with a Varian 4-mm double-resonance T3 solid probe for the ^{13}C nuclei and a 40-ms acquisition period with an 86-kHz ^{1}H decoupling radio frequency with a small phase incremental alteration (SPINAL) decoupling pulse sequence.[19] The cross-polarization/magic angle spinning (CP–MAS) NMR spectra were measured with a ramped-amplitude pulse sequence[20] with a 2-ms contact time and a 2.6-μs $\pi/2$ pulse for the ^{1}H nuclei over a temperature range of −30 to 100°C. The amplitude of the ^{1}H nuclei ramping down linearly from 92.6% of its final value was used during the cross-polarization contact time. The spectra were collected over a 30.7-kHz spectral width with a 5.0-s recycle delay in 256 transients (singal-noise ratio > 98). The contact time was optimized by the measurements of several selected samples with variable contact times (100–8000 μs). Fiber samples were cut and placed in zirconium rotors 4 mm in diameter, which were spun at the magic angle at 15 kHz subsequently.

The ^{1}H spin-lattice relaxation time (T_1H) was indirectly measured via the detection of the ^{13}C resonance and enhanced by the cross-polarization applied after a π pulse to the ^{1}H nuclei with the inversion recovery method. The ^{13}C spin-lattice relaxation time (T_1C) was measured with the conventional Torchia's pulse sequence.[21] The relaxation time analyses were performed with the same solid-state probe with the same contact time and acquisition period used for the CP–MAS ^{13}C-NMR spectrum.

RESULTS AND DISCUSSION

Intercalative polymerization

Figure 1 gives an outline of the reactive extrusion-molding machine used in the experiment. The machine consisted of a mixing hopper (the first step) and a single-screw extruder (the second step). The mixing hopper was equipped with a shuttlecock-type screw, which enabled the stirring of solid mixtures and/or liquid samples under applied heat. A 30-mm single-screw extruder (length/diameter = 15) was connected with the mixing hopper through a gear pump. Because the collection entrance was located under the gear pump and terminal of the extruder, both one- and two-step reactions were possible with the reactive extrusion-molding machine.

The effect of changing the D18 cation mixing ratio in D18Mt was examined with the two-step method.

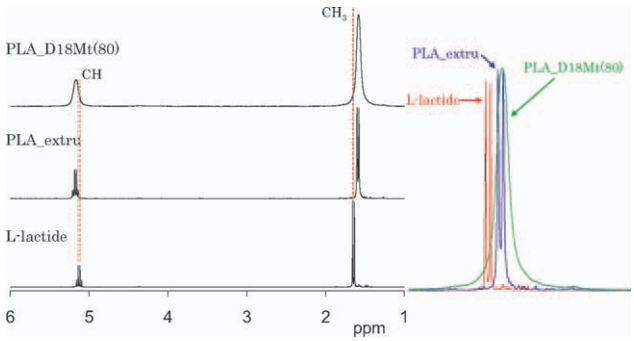

Figure 2 ^{1}H-NMR spectra of the L-lactide, PLA homopolymer (PLA_extru), and PLA/clay nanocomposite [PLA_D18Mt(80)] (left) and an enlarged view of the CH_3 area (right). [Color figure can be viewed in the online issue, which is available at wileyonlinelibrary.com.]

Reaction samples of L-lactide with different D18 amounts in D18Mt were collected from the exit of the single-screw extruder. The polymerization and extrusion were performed under a nitrogen atmosphere or vacuum conditions. Regardless of the amount of D18, solidified fiber samples (M_n = 22,500–23,500) were obtained with the spinning roll. The unreacted L-lactide was trapped before the vacuum pump and accompanied by existing water in the molding. Figure 2 shows the changes in the ^{1}H-NMR spectra in $CDCl_3$ before and after polymerization and with and without D18Mt. The CH_3 peaks of L-lactide shifted to high field, and the CH peaks shifted downfield after polymerization (PLA_extru: PLA homopolymer made by the reactive extrusion-molding). In the presence of D18Mt, line broadening was observed due to paramagnetic impurities of Fe^{3+}. Judging from the chemical shift and symmetry of the ^{1}H peaks of PLA_D18Mt(80), little L-lactide existed in the fiber samples. The relatively lower M_n of the PLA/clay nanocomposite was probably caused not only by hydroxyl groups at the surface of the clay but also by bound water. The results of the thermal analyses are summarized in Table I. With the addition of D18Mt, the T_c values of the fiber samples decreased slightly, although the T_g and T_m values of these samples were similar to those of PLA_extru. The T_{dec} values of the fiber samples increased slightly with the addition of D18Mt; the PLA/clay nanocomposite with D18Mt(80) had a higher T_{dec} value than the composites with D18Mt(60) and D18Mt(100). Generally, the organo-Mts slightly affected the thermal properties of the PLA chain with only 3 wt % additions.

TABLE I
Molecular Weight (M_n) and Thermal Properties of the PLA/Clay Nanocomposites

		DSC			TGA
Sample	M_n	T_g (°C)	T_c (°C)	T_m (°C)	T_{dec} (°C)
PLA	2.42×10^4	52	87	166	260
PLA_DMt(60)	2.35×10^4	53	85	165	270
PLA_DMt(80)	2.25×10^4	51	83	163	278
PLA_DMt(100)	2.31×10^4	51	82	165	272

TABLE II
Interlayer Distances of the Montmorillonites and PLA/Clay Nanocomposites

	X-ray	
Sample	Peak/2θ	d_{001} (nm)
D18Mt(60)	3.4	2.6
D18Mt(80)	3.2	2.8
D18Mt(100)	2.9	3.0
PLA_DMt(60)	2.5	3.5
PLA_DMt(80)	2.5	3.5
PLA_DMt(100)	2.5	3.5

Characterization of the PLA/clay nanocomposites

To study the composite morphology, X-ray diffraction (XRD) analysis was performed on the starting organo-Mts and the PLA/clay nanocomposites; the results are shown in Table II. Although the interlayer distances of organo-Mts increased with the D18 content, the interlayer distances of the PLA/clay nanocomposites remained the same, despite the D18 content; this implied that the amount of D18 had little influence on the morphology of the PLA/clay nanocomposite.

Next, to evaluate the performance of the reactive extrusion molding and to analyze the production process further, we compared samples collected before and after extrusion with XRD, mechanical property tests, SEM, and TEM analyses. Figure 3 shows the XRD patterns of D18Mt(80) (the organo-

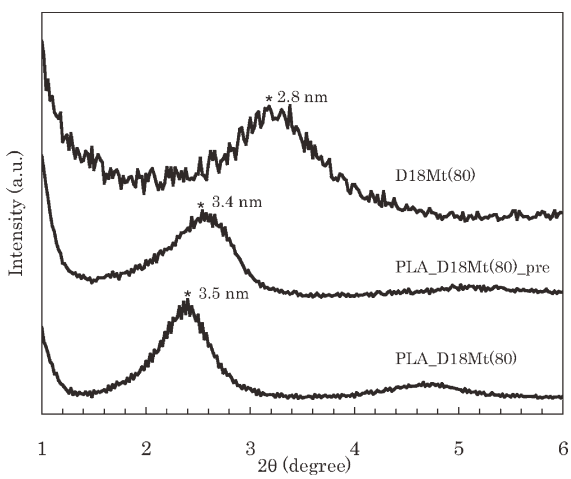

Figure 3 XRD patterns of D18Mt(80), PLA_D18Mt(80)_pre, and PLA_D18Mt(80). The interlayer distance is designated by an asterisk.

TABLE III
Tensile Properties of the PLA/Clay Nanocomposites

	Tensile strength (MPa)	Elongation at break (%)	Tensile elastic modulus (MPa)
PLA_DMt(80)_pre	35.2 ± 4.5	2.64 ± 0.50	1674 ± 122
PLA_DMt(80)	45.0 ± 0.9	3.62 ± 0.17	1352 ± 137

Mts), PLA_D18Mt(80)_pre (the one-step reaction sample, collected before extrusion), and PLA_D18Mt(80) (the two-step reaction sample, collected after extrusion). The peak angle was already shifted toward the lower 2θ region even before the extrusion. The interlayer distances of D18Mt(80)–PLA_D18Mt(80)_pre–PLA_D18Mt(80), given as two-digit numbers with an asterisk in Figure 3, showed a little change before and after the extrusion: 2.8–3.4–3.5 nm, respectively. This enlargement of the interlayer distances indicated that even in the sample before extrusion, the PLA polymer chain was introduced between the clay layers; this led to an intercalated morphology. The results of the tensile tests of PLA_D18Mt(80)_
pre and PLA_D18Mt(80) are summarized in Table III. After the extrusion, the mechanical properties of the fiber were improved: the tensile strength increased, whereas the tensile elastic modulus decreased. Figure 4 shows typical SEM images of PLA_D18Mt(80)_pre and PLA_D18Mt(80); agglomerated particles were observed in PLA_D18Mt(80)_pre, whereas through the extrusion process, these structural defects disappeared, and a fine microstructure was formed in the PLA_D18Mt(80). This resulted in an improved dispersion. The morphology of the PLA/clay nanocomposites was also confirmed by TEM. Figure 5 shows typical high-magnification TEM images of PLA_D18Mt(80)_pre and PLA_D18Mt(80); intercalated clay tactoids without exfoliated single platelets can be found in both images. Although small parts of the clay platelets (3–5 stacks) separated from the tactoids in part were observed in the image of PLA_D18Mt(80), no exfoliated single platelets existed in any of the observation fields.

To summarize the characterizations results, intercalative polymerization proceeded immediately in the mixing hopper (the first step); then, further dispersion occurred in the single-screw extruder (the second step). The PLA/clay nanocomposite took on the intercalated morphology both in the mixing hopper and in the single-screw extruder. Although structural defects decreased and the dispersion was improved by the reactive extrusion molding, the single-screw extruder did not have the mixing ability to form a composite consisting solely of the exfoliate morphology.

Solid-state NMR spectra

On the basis of the previous knowledge of the morphology and dispersion of the PLA/clay nanocomposite, solid-state NMR was used to analyze the molecular mobility and structural changes as a function of temperature in the range that included T_g and T_c. For the PLA samples with and without organo-Mts and containing different amounts of D18, CP–MAS ^{13}C-NMR spectra were measured at different temperatures. For typical examples, the spectra of PLA_extru and PLA_D18Mt(80) showed similar peak shapes with increases in temperature, as shown in Figure 6; the peak intensity of each material decreased due to a reduction in the efficiency of the ^{1}H–^{13}C cross-polarization. Particularly near and above the T_c point, the signal strength explicitly decreased and the shape of CH and C=O peaks changed to asymmetrical; this was obtained by the addition of small crystalline peaks[22] into the symmetrical amorphous ones. On the other hand, no asymmetrical shapes about the CH and C=O peaks were observed below the T_g point; this suggested

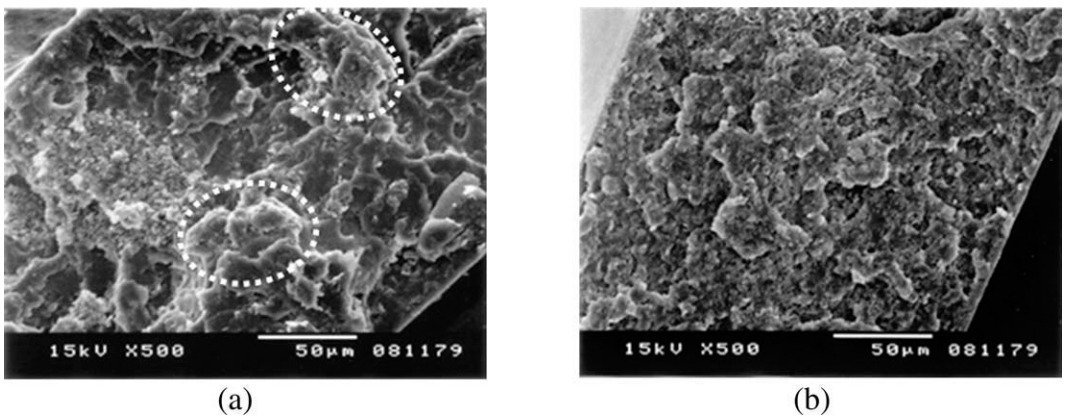

Figure 4 SEM micrographs of the PLA/clay nanocomposites: (a) PLA_D18Mt(80)_pre (left) and (b) PLA_D18Mt(80) (right). The dotted circles show the aggregates.

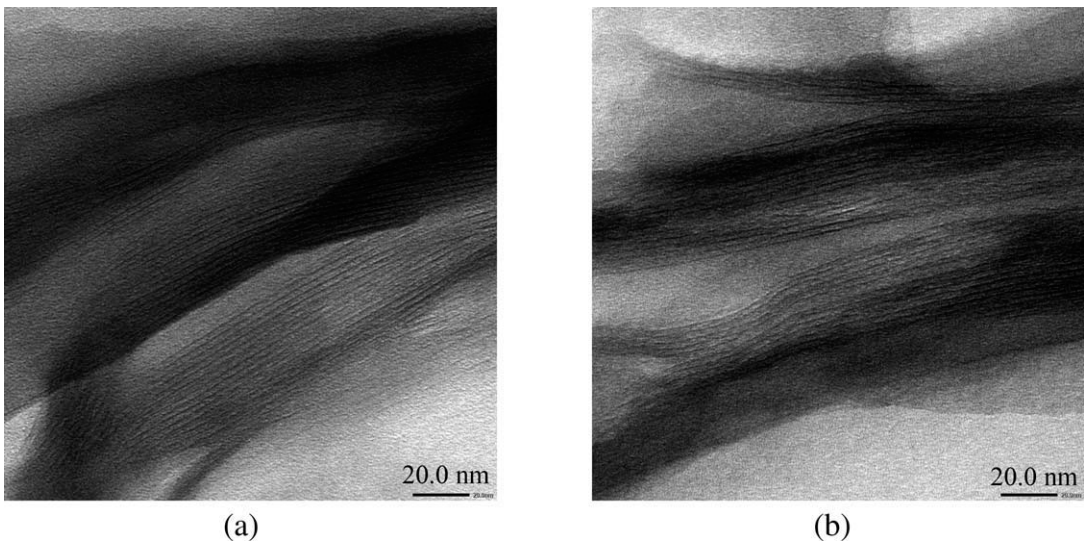

Figure 5 TEM micrographs of the PLA/clay nanocomposites: (a) PLA_D18Mt(80)_pre (left) and (b) PLA_D18Mt(80) (right).

that the polymer was amorphous. These changes in the peak patterns appeared in almost all of our PLA/clay nanocomposites, regardless of the D18 content of organo-Mts.

To investigate the behaviors of the macromolecules near the T_g and T_c points, relaxation time analysis was performed on (1) five samples produced by reactive extrusion molding, as shown previously

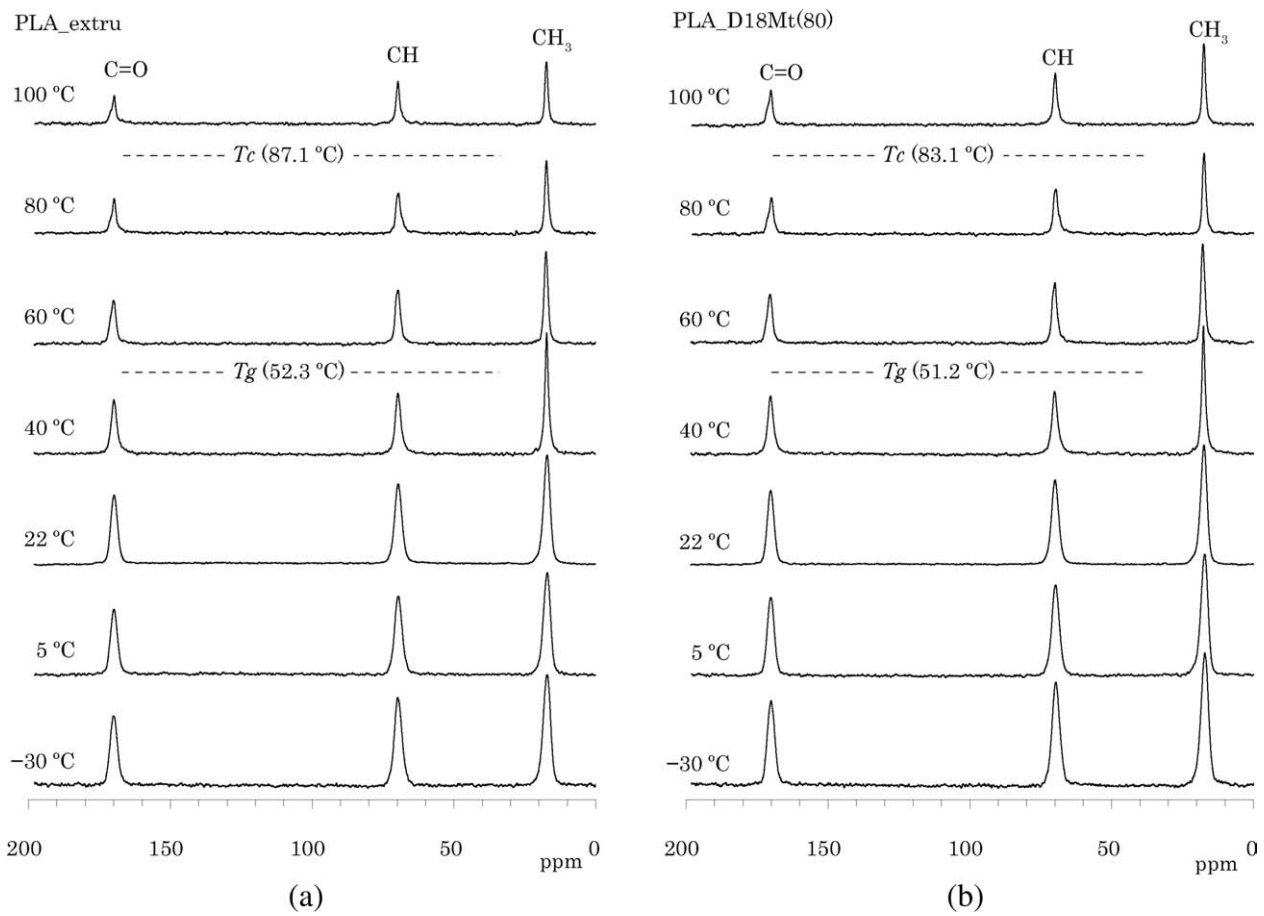

Figure 6 CP–MAS ^{13}C-NMR spectra of the PLA homopolymer (PLA_extru) and the PLA/clay nanocomposite [PLA_D18Mt(80)] at different temperatures.

[PLA_extru, PLA_D18Mt(60), PLA_D18Mt(80), PLA_D18Mt(100), and PLA_D18Mt(80)_pre], (2) commercially available PLA (PLA_ref), and (3) a mixture of 3 wt % D18Mt(80) and PLA_ref in a plastic bag [PLA_D18Mt(80)_mix].

T_1H analysis

In the indirect determination of T_1H by CP–MAS ^{13}C-NMR measurements, T_1H values determined with any of the carbon peaks were generally almost the same because of the spin diffusion of ^1H nuclei. Plots of the T_1H values calculated with the CH and CH_3 peaks versus reciprocal temperature are shown in Figures 7 and 8, respectively. For all of the T_1H graphs, the error bars indicate standard errors in the regression calculation. It was considered that larger standard errors above 80°C were caused by a lower efficiency of the cross-polarization and formation of the crystal phase. In a comparison of Figures 7 and 8, the T_1H values determined between the CH and CH_3 peaks showed a similar tendency. In all of the measured samples, the T_1H values increased with temperature. Recent research on the T_1H values of PLA composites found that more well-dispersed exfoliated composites exhibited lower T_1H values.[23] In the composites with less dispersed morphologies, that is, intercalated and microcomposite forms, the decrease in the T_1H values was small.[24,25] All of the extruded samples had similar T_1H values below room temperature, and all showed increasing T_1H with increases in temperature. However, the increase was lower in the PLA/clay nanocomposites than in PLA_extru above room temperature in Figs. 7(a) and 8(a) [10^3/(absolute temperature) < 3.4]. Regardless of the D18 content of organo-Mts, the T_1H values of the three PLA/clay nanocomposites were almost the same, even for different temperatures in the range of −30 to 100°C. As shown in Figure 7(b) and 8(b), in the case of PLA_D18Mt(80)_pre (the one-step sample collected before extrusion), we also observed suppression of the increase in T_1H values compared with PLA_extru above room temperature. With regard to other PLA homopolymers

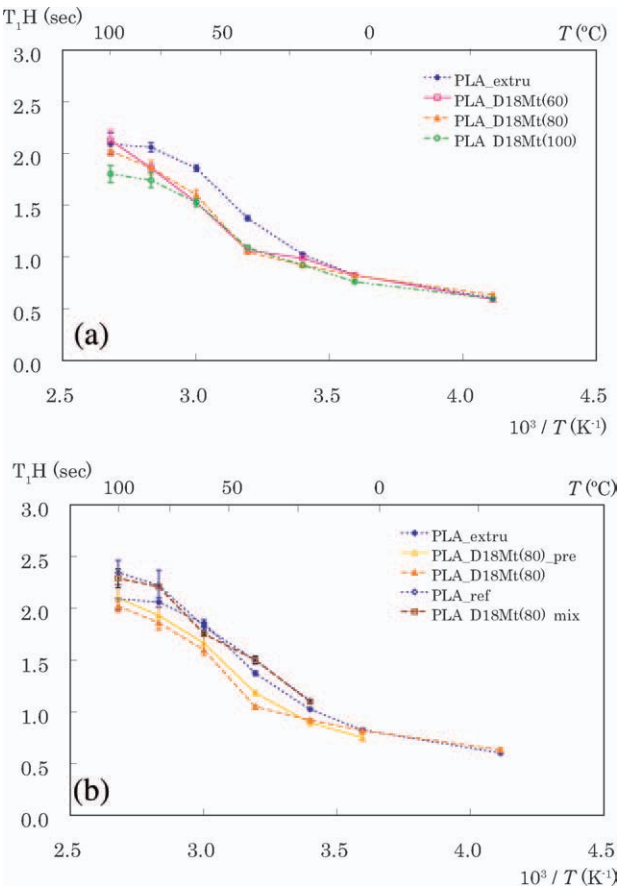

Figure 7 Plot of the T_1H values of the CH group versus the reciprocal temperature with various (a) D18 contents (upper) and (b) morphologies (bottom). The error bars indicate the standard errors in the regression calculation. [Color figure can be viewed in the online issue, which is available at wileyonlinelibrary.com.]

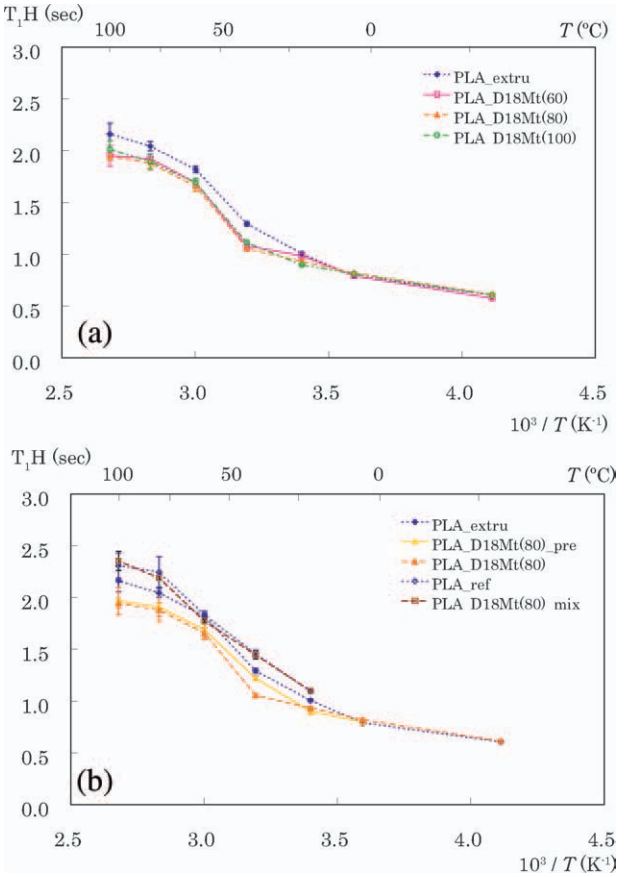

Figure 8 Plot of the T_1H values of the CH_3 group versus the reciprocal temperature with various (a) D18 contents (upper) and (b) morphologies (bottom). The error bars indicate the standard errors in the regression calculation. [Color figure can be viewed in the online issue, which is available at wileyonlinelibrary.com.]

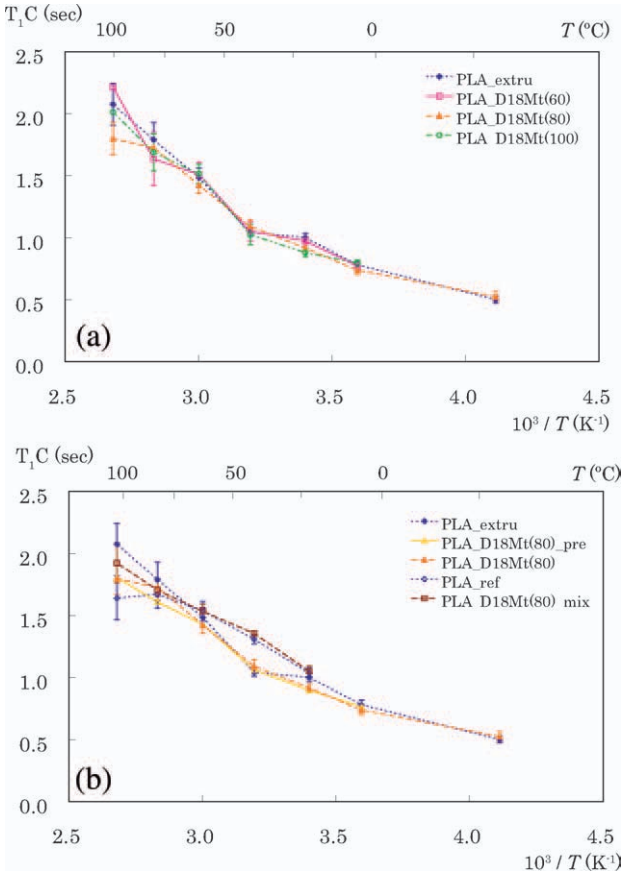

Figure 9 Plot of the T_1C values of the CH_3 group versus the reciprocal temperature with various (a) D18 contents (upper) and (b) morphologies (bottom). The error bars indicate the standard errors in the regression calculation. [Color figure can be viewed in the online issue, which is available at wileyonlinelibrary.com.]

having different T_g and M_n values, PLA_ref (having higher M_n) had longer T_1H values, with the exception of its T_g point. Furthermore, the T_1H value of the simply mixed sample, PLA_D18Mt(80)_mix, exhibited no difference from the original PLA, PLA_ref. The reason for these results was probably that the extruded samples had a lower T_g point and smaller M_n than the commercially available PLA.

T_1C analysis

T_1C was examined with Torchia's pulse sequence. Plots of the T_1C values calculated by the CH_3 peaks versus the reciprocal temperature are shown in Figure 9. The experimentally obtained curves of the T_1C values of CH_3 showed a similar tendency to those of T_1H. Their standard errors above 80°C were, however, larger than those of T_1H. The T_1C values of CH_3 of the PLA/clay nanocomposite were similar to those of PLA_extru without suppression of the increase in T_1C values compared with PLA_extru above room temperature [Fig. 9(a)]. On the other hand, the PLA_ref and PLA_D18Mt(80)_mix samples had similar T_1C values of CH_3, which were higher than those of PLA_extru and the PLA/clay nanocomposites in the range 22–60°C [Fig. 9(b)], unlike the T_1H values.

The trends in T_1C of the backbone carbon were different from that of the CH_3 group. Figures 10 and 11 show plots of the T_1C values calculated from the CH and C=O peaks, respectively, versus the reciprocal temperature. Shown as error bars in the figures, the standard errors in the regression calculation of the T_1C values of CH and C=O were larger even below 60°C compared with those of the T_1C values of CH_3 and the T_1H values. These errors of the data fitting may have been caused by the longer T_1C values and the contribution of multiple relaxations. Thus, we discuss the T_1C values of CH and C=O with consideration of the error margins. In all of the PLA compounds, with an increase in

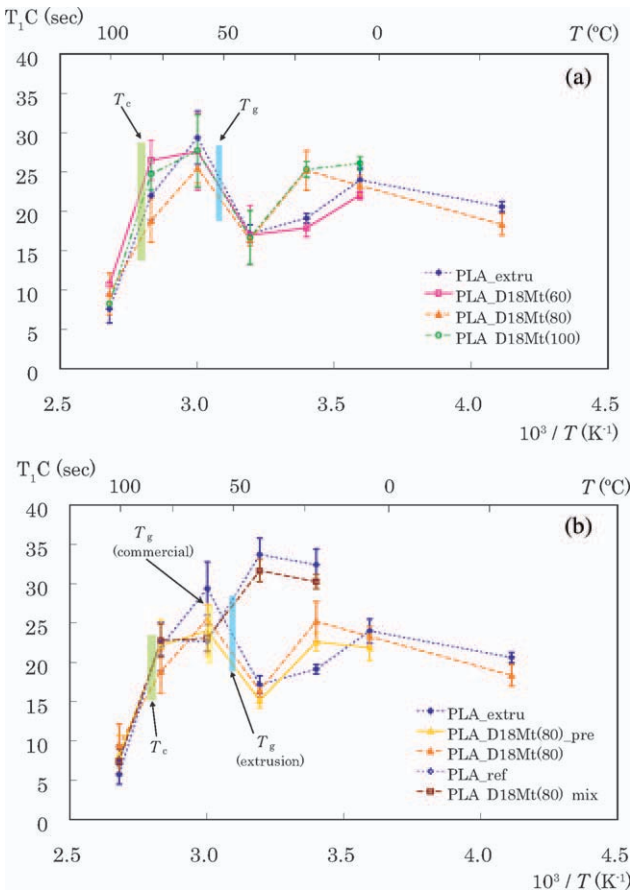

Figure 10 Plot of the T_1C values of the CH group versus the reciprocal temperature with various (a) D18 contents (upper) and (b) morphologies (bottom). The error bars indicate the standard errors in the regression calculation. [Color figure can be viewed in the online issue, which is available at wileyonlinelibrary.com.]

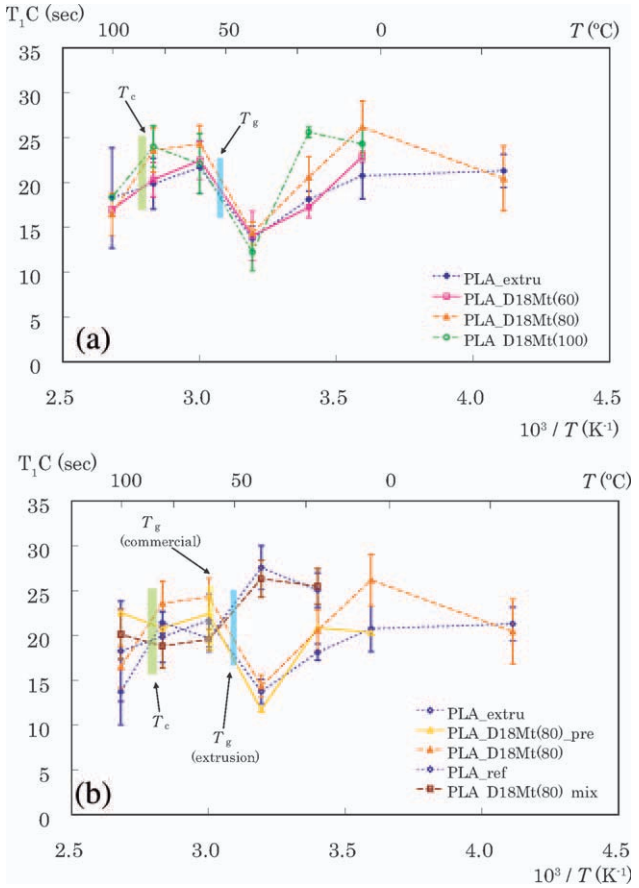

Figure 11 Plot of the T_1C values of the C=O group versus the reciprocal temperature with various (a) D18 contents (upper) and (b) morphologies (bottom). The error bars indicate the standard errors in the regression calculation. [Color figure can be viewed in the online issue, which is available at wileyonlinelibrary.com.]

temperature, the T_1C values of both the CH and C=O groups reached minimal values and were then significantly reduced, except the unclear minimal T_1C values of the C=O groups for PLA_ref and PLA_D18Mt(80)_mix (the T_g and T_c points are indicated in Figs. 10 and 11), whereas the T_1C values of the CH_3 group (Fig. 9) monotonically increased with increasing temperature. The temperature at the T_1C minimum was not affected by the addition of organo-Mts but was affected by the T_g value and/or molecular weight: no change in the minimal T_1C value was observed between the extruded PLA and the composite (ca. 40°C), as shown in Figure 10(a). The effect of the PLA/clay nanocomposite appeared as an increase in the T_1C value for samples with more than 80% D18; the T_1C values generally increased around room temperature [Figs. 10(a) and 11(a)]. Meanwhile, at temperatures above T_g, rapid decreases in the T_1C values of the CH group were observed. The alternation of molecular motion of the backbone was one reason for the rapid decline.[26] We considered that this alternation of molecular motion also caused divergences of the T_1C tendency in the CH groups above T_g.

Relaxation time analyses

It was considered that the relaxations of the ^1H nuclei and ^{13}C nuclei of the CH_3 groups mainly occurred through the motion of CH_3 in the extreme narrowing region.[27,28] On the other hand, it has been reported that the paramagnetic Fe^{3+} of clay influenced the polymer protons near the clay surface.[24] According to the previous discussions, in our case, the addition of organo-Mts into the PLA matrix did not suppress the motion of CH_3 but accelerated the relaxation of the H nuclei to the clay. Thus, in the samples formed by extrusion, the T_1C value of CH_3 was not changed, but the T_1H value decreased compared with that of the original PLA_extru. In contrast, the T_1C values of CH and C=O exhibited the minimal value near the T_g point followed by a drastic increase [Figs. 10(a) and 11(a)]. This enabled us to explain the relaxation time changes that appeared in the particular temperature range including the T_g point as the boundary. To validate our results, however, more studies on the magnetic relaxation are necessary that employ compounds based on the PLA that have different environments. Our planned future work includes an investigation of the molecular dynamics and relaxation times of other PLA compounds.

CONCLUSIONS

Melt polymerization was adopted to produced PLA/clay nanocomposites starting from L-lactide and organically modified montmorillonite. The melt polymerization used a reactive extrusion-molding process and employed a mixing hopper and a single-screw extruder. It was found by XRD, SEM, and TEM analyses that almost all of the PLA polymer chains were constructed with an intercalated morphology in the mixing hopper; this was followed by dispersion on the micrometer scale in the single-screw extruder. When the composite was made and mixed with the organoclay, there were few changes in the CP–MAS ^{13}C-NMR spectra, even over a temperature range from −30 to 100 °C. The T_1H values above room temperature were reduced by this intercalated morphology of the PLA/clay nanocomposite, whereas no suppression was observed by simple mixing with the organoclay. The intercalated morphology also affected the T_1C values: the organoclay accelerated the relaxation from the ^{13}C nuclei of the CH_3 group and depressed the relaxation from the backbone of PLA. In almost all of the PLA compounds we analyzed, the minimum T_1C values for both the CH

and C=O groups appeared at 40°C and a significant reduction of these value was observed above the T_c point.

The authors wish to express special thanks to Yoshikazu Fujita, Nagoya University, for help with the TEM sample preparation and operation.

References

1. Bordes, P.; Pollet, E.; Avrous, L. Prog Polym Sci 2009, 34, 125.
2. Maiti, P.; Yamada, M.; Okamoto, M.; Ueda, K.; Okamoto, K. Chem Mater 2002, 14, 4654.
3. Ray, S. S.; Okamoto, M. Prog Polym Sci 2003, 28, 1539.
4. Ahmadi, S. J.; Huang, Y. D.; Li, W. J Mater Sci 2004, 39, 1919.
5. Pavlidoua, S.; Papaspyrides, C. D. Prog Polym Sci 2008, 33, 1119.
6. Ray, S. S.; Yamada, K.; Ogami, A.; Okamoto, M.; Ueda, K. Macromol Rapid Commun 2002, 23, 943.
7. Ray, S. S.; Yamada, K.; Okamoto, M.; Ogami, A.; Ueda, K. Chem Mater 2003, 15, 1456.
8. Li, B.; Dong, F. X.; Wang, X. L.; Yang, J.; Wang, D. Y.; Wang, Y. Z. Eur Polym J 2009, 45, 2996.
9. Thellen, C.; Orroth, C.; Froio, D.; Ziegler, D.; Lucciarini, J.; Farrel, R.; D'souza, N. A.; Ratto, J. A. Polymer 2005, 46, 11716.
10. Paul, M. A.; Delcourt, C.; Alexandre, M.; Degée, P.; Henrist, C.; Rulmont, A.; Dubois, P. Polymer 2003, 44, 443.
11. Shim, J. H.; Kim, E. S.; Joo, J. H.; Yoon, J. S. J Appl Polym Sci 2006, 102, 4983.
12. Lin, L. H.; Liu, H. J.; Yu, N. K. J Appl Polym Sci 2007, 106, 260.
13. Paul, M.-A.; Delcourt, C.; Alexandre, M.; Degée, P.; Monteverde, F.; Rulmont, A.; Dubois, P. Macromol Chem Phys 2005, 206, 484.
14. Paul, M. A.; Alexandre, M.; Degée, P.; Calberg, C.; Jérôme, R.; Dubois, P. Macromol Rapid Commun 2003, 24, 561.
15. Nijenhuis, A. J.; Gripma, D. W.; Pennings, A. J. Macromolecules 1992, 25, 6419.
16. Stevels, W. M.; Bernard, A.; Van de Witte, P.; Dijkstra, P. J.; Feijen, J. J Appl Polym Sci 1996, 62, 1295.
17. Yamaguchi, T.; Yamada, E. Polym Int 2006, 55, 662.
18. Yamaguchi, T.; Yamada, E. e-J Soft Mater 2006, 2, 1.
19. Fung, B. M.; Khitrin, A. K.; Ermolaev, K. J Magn Reson 2000, 142, 97.
20. Metz, G.; Wu, X. L.; Smith, S. O. J Magn Reson A 1994, 110, 219.
21. Torchia, D. A. J Magn Reson 1978, 30, 613.
22. Thakur, K. A. M.; Kean, R. T.; Zupfer, J. M.; Buehler, N. U.; Doscotch, M. A.; Munson, E. J. Macromolecules 1996, 29, 8844.
23. Bourbigot, S.; Fontaine, G.; Bellayer, S.; Delobel, R. Polym Test 2008, 27, 2.
24. Bourbigot, S.; Vanderhart, D. L.; Gilman, J. W.; Awad, W. H.; Davis, R. D.; Morgan, A. B.; Wilkie, C. A. J Polym Sci Part B: Polym Phys 2003, 41, 3188.
25. Bourbigot, S.; Vanderhart, D. L.; Gilman, J. W.; Bellayer, S.; Strets, H.; Paul, D. R. Polymer 2004, 45, 7627.
26. Kikuchi, H.; Tokumitsu, H.; Seki, K. Macromolecules 1993, 26, 7326.
27. Kurosu, H.; Yamada, T.; Ando, I.; Sato, K.; Otsu, T. J Mol Struct 1993, 300, 303.
28. Lyerla, J. R.; Yannoni, C. S.; Fyfe, C. A. Acc Chem Res 1982, 15, 208.